DOI: 10.13009/EUCASS2023-381
Aerospace Europe Conference 2023 – 10TH EUCASS – 9TH CEAS

Numerical Analysis on the Combustion Behavior Varying with Equivalence Ratio in a GO_2-GCH_4 Combustor

Hong Yeong Park, Yun Hyeong Kang*, Jae Won Lee**, Jong Hyun Kim** and Jeong Soo Kim*†*
**Pukyong National University, Department of Mechanical Engineering*
48513 BUSAN, Republic of Korea
***Hanhwa Aerospace Co., Ltd.*
34101 Daejeon, Republic of Korea
hypark@pukyong.ac.kr– yhkang@pukyong.ac.kr– cfdljw@hanwha.com–
jonghyunk@hanwha.com – jeongkim@pknu.ac.kr
† Corresponding Author

Abstract
Numerical calculation was performed to simulate the combustion behavior of a GO_2-GCH_4 combustor varying with equivalence ratio under the fuel-rich conditions. The diffusion flamelet model was applied to the calculations. The equivalence ratio of 2 to 3.65 was calculated in a steady state to compare the flow structure, but the equivalence ratio of 5.36 was analyzed in a transient state to observe the variation of characteristic velocity over time. As a result, it was founded that the thrust and combustion performance calculated by the simulations were in good agreement with the experimental results. However, it was observed that the combustion model cannot predict unsteady physics. In order to realize these phenomena, further research will be conducted.

1. Introduction

As the space industry evolves, the demand for cost reduction and eco-friendliness increases with the frequency of the rocket launches. Methane, the representative green fuel, is not only efficient and reliable, but also produces less pollutants during combustion. Methane is also becoming increasingly popular as a propellant for space exploration, with the potential for ISRU (In-Situ Resource Utilisation) on Mars[1].

In particular, the LOx-methane has been shown to have superior performance in terms of specific impulse compared to the LOx-kerosene, as asserted by many research[1,2]. Methane is also more cost effective, being less than one third of kerosine's price. Additionally, it has the advantage of higher density compared to liquid hydrogen, making it excellent for storage. For these reasons, advanced countries in space development such as the United States, Russia, Europe, and Japan have adopted Methane as the propellant for next generation launch vehicles.

To develop an engine with optimal performance, it is crucial to have information about combustion efficiency and ignition stability based on propellant supply conditions. However, methane has a relatively short development history, resulting in limited experimental data. Overcoming the lack of such information requires conducting tests under various operating conditions, which can be time-consuming, costly, and associated with risks. On the other hand, numerical analysis makes it possible to model and analyze chemical reactions under various combustion conditions that are difficult to achieve by experimental approaches alone. It allows important design factors to be determined in advance, significantly reducing development time and cost. In addition, using validated computational method, numerical analysis can provide information on temperature and turbulence characteristics within the combustion chamber that are difficult to obtain directly from experiments.

In this study, prior to analysing the combustion behavior of a LOx-GCH_4 small rocket engine, a numerical analysis was performed to establish a method capable of predicting combustion behavior of rocket engines. The objective was to simulate the behavior of a GO_2-GCH_4 combustor varying with equivalence ratio under the fuel-rich conditions. The constructed analysis model was validated by comparing the calculated thrust and combustion performance results with experimental data from in-house hot-firing tests. The flow structure inside of the combustion chamber was observed through the results of numerical analysis.

DOI: 10.13009/EUCASS2023-381

2. Experiment case descriptions

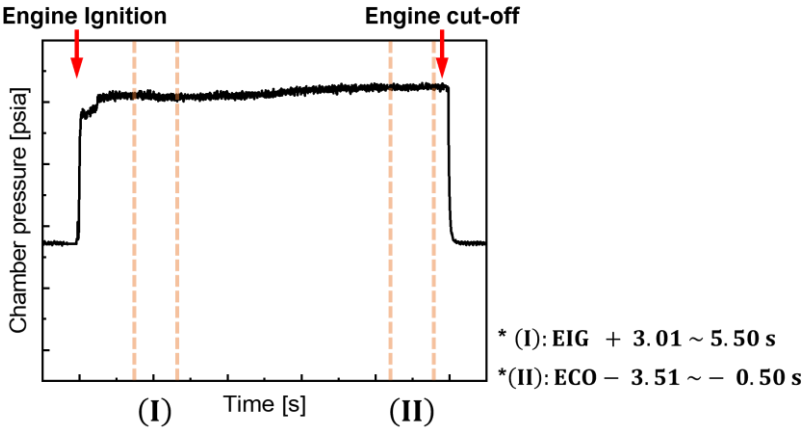

Figure 1: Two sections where data was obtained in the combustion duration.

Table 1: Experimental cases used in the calculations.

Equivalence ratio[a]	Relative rise of C*[b] [%]	(I)	(II)
2.00	0.06	GE1.1	GE1.2
2.97	1.28	GE4.1	GE4.2
3.65	2.17	GE6.1	GE6.2
5.36	6.28	GE11	

[a] $\phi = (MR)_{F/O}/(MR)_{Stoich}$ [b] $C^*_{RR} = (C^*_{II} - C^*_I)/\ C^*_I \times 100$

The ground hot-firing test conducted as a part of the development process for a small rocket engine using methane-oxygen aimed to verify the combustion performance of the GO_2-GCH_4 combustor under the fuel-rich conditions[3]. Mass flow rate of GO_2 was fixed at 12 g/s, therefore equivalence ratio was determined by the mass flow rate of GCH_4. Two periods within the combustion duration were set as shown in Figure 1 to compare the changes in combustion characteristics over the period. Period (I) was set from 3.01 to 5.5 seconds after engine ignition (EIG, Engine Ignition), and period (II) was set during the 3 seconds before the propellant supply valve closed (ECO, Engine Cut-off). Through the tests, it was observed that as the equivalence ratio increased, there was a distinct rise of the characteristic velocity in the later stage (period II) of the firing duration. This phenomenon was attributed to the strengthened chemical reaction caused by the re-participation of incomplete combustion products or unburned mixture components that did not participate at the initial stage of combustion. Table 1 summarizes the experimental cases, comprised of equivalence ratios and the relative rise of characteristic velocity which were used for the comparison with analysis. The equivalence ratio of 2 to 3.65 was analyzed in a steady state to observe the internal flame structure affected by equivalence ratio, while the case with the highest rate of change in characteristic velocity, equivalence ratio of 5.36, was simulated in a transient state to observe the variations in pressure and characteristic velocity over time.

3. Numerical setup

The internal flow field of the combustion chamber was analyzed using the RANS (Reynolds-Averaged Navier-Stokes) equations, using the commercial code Ansys Fluent 2021 R1[4]. The geometric model for the analysis was constructed as a two-dimensional axisymmetric one, and the computational domain was set from the injector face to the nozzle exit. To improve convergence during the analysis, a pressure-based coupled algorithm was adopted. Governing equations were discretized using a second-order upwind scheme for all cases, except the transport equation of turbulent scalar.

DOI: 10.13009/EUCASS2023-381

3.1 Turbulence model

To analyze turbulent flow, the compressible standard k-ε model[5,6] was utilized, with the compressibility effects being considered. The turbulent kinetic energy (k) and turbulent dissipation rate (ε) were derived using Eq. (1) and (2), respectively. The turbulent viscosity can be expressed as shown in Eq. (3). The time derivatives of each equation are not considered in the steady-state analysis.

$$\frac{\partial k}{\partial t}+\frac{\partial(\rho k u_i)}{\partial x_i}=\frac{\partial}{\partial x_j}\left[\left(\mu+\frac{\mu_t}{\sigma_k}\right)\frac{\partial k}{\partial x_j}\right]+G_k-\rho\varepsilon(1+M_T) \tag{1}$$

$$\frac{\partial \varepsilon}{\partial t}+\frac{\partial(\rho \varepsilon u_i)}{\partial x_i}=\frac{\partial}{\partial x_j}\left[\left(\mu+\frac{\mu_t}{\sigma_\varepsilon}\right)\frac{\partial \varepsilon}{\partial x_j}\right]+C_{1\varepsilon}\frac{\varepsilon}{k}G_k-C_{2\varepsilon}\rho\frac{\varepsilon^2}{k} \tag{2}$$

$$\mu_t=\rho C_\mu\frac{k^2}{\varepsilon} \tag{3}$$

Where, $G_k=-\rho\overline{u_i'u_j'}\frac{\partial u_j}{\partial x_i}$, $M_T^2=\frac{2k}{a^{2'}}$, $C_{1\varepsilon}=1.44$, $C_{2\varepsilon}=1.92$, $C_\mu=0.09$, $\sigma_k=1.0$, $\sigma_\varepsilon=1.3$ and ρ is the density.

The compressible standard k-ε turbulence model incorporates a pressure-dilatation term in the equation of turbulent kinetic energy, allowing for the consideration of turbulent energy reduction with increasing Mach numbers. This feature enhances the predictive performance of turbulent flow[7]. To improve the accuracy of flow near the wall, the enhanced wall treatment is selected as the wall function model[8]. It aims to provide better accuracy in the flow near the wall region.

3.2 Combustion model

The non-adiabatic diffusion flamelet[9], a type of non-premixed combustion model, was employed in this calculation. The diffusion flamelet model assumes the turbulent flame field as a collection of one-dimensional laminar flamelets and is analyzed accordingly. The micro-structure of flame is governed by the scalar dissipation rate[10]. The partial differential equations in one-dimension for the non-adiabatic diffusion flamelet are derived under the assumption that all chemical species have the same diffusion coefficients. They are defined by Eq. (4) and (5) as shown below.

$$\frac{\partial Y_i}{\partial t}=\frac{\chi}{2}\frac{\partial^2 Y_i}{\partial t^2}+\frac{\dot{\omega}_i}{\rho} \tag{4}$$

$$\frac{\partial T}{\partial t}=\frac{\chi}{2}\frac{1}{C_P}\frac{\partial^2 h}{\partial Z^2}-\frac{\chi}{2}\frac{1}{C_P}\sum_{k=1}^{N}h_k\frac{\partial^2 Y_k}{\partial Z^2}-\frac{1}{\rho C_P}\dot{\omega}_t \tag{5}$$

Where, Y_i is the mass fraction of i-th species of mixture, $\dot{\omega}_i$ the mass production rate of i-th species of mixture, T the temperature, C_P the specific heat at constant pressure, h the enthalpy of mixture, Z the mixture fraction, $\dot{\omega}_t$ the energy source term and χ is the scalar dissipation rate, described as $\chi=2D\left(\frac{\partial Z}{\partial x_i}\right)^2$.

For simulating the combustion reactions of methane and oxygen, The DRM-19 mechanism was employed, which includes 21 chemical species and 84 reactions[11]. The DRM-19 mechanism is a reduced model derived from the GRI-mech 1.2, which provides a good representation of the thermodynamic characteristics of methane combustion while reducing computational costs. Particularly for methane-oxygen combustion, it has been reported that the predicted burning velocity from DRM-19 aligns well with experimental results[12].

DOI: 10.13009/EUCASS2023-381

Table 2: Boundary conditions used in the calculation.

Boundary	Type	Specification
GO_2/GCH_4 inlet	Mass-flow rate	T= 298 K
Injector faceplate	Wall	No slip, adiabatic
Combustion chamber wall	Wall	Temperature profile
Axis	Axisymmetric	-

3.3 Boundary conditions

Table 2 summarizes the boundary conditions used in the calculations. For the inlet condition, the mass-flow rates obtained from experimental measurements were used, and the pressure boundary condition was applied at the nozzle exit. The temperature values of methane and oxygen at the inlet were assumed to be 298 K each, and the injector face, excluding the propellant injection region, was assigned adiabatic and no-slip condition. Since the temperature values were measured only up to the lower part of the combustion chamber, the temperatures of the nozzle throat and outlet were additionally calculated with the NASA CEA (Chemical Equilibrium with Application) code[13] to set the overall temperature profile for combustor wall condition.

3.4 Sensitivity analysis for grid system

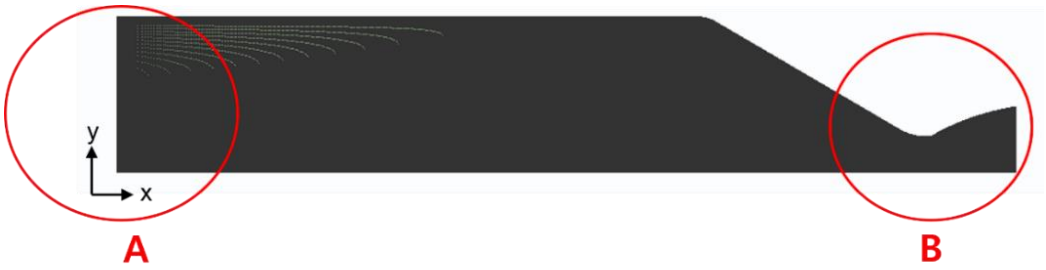

Figure 2: Grid system in the full computational domain.

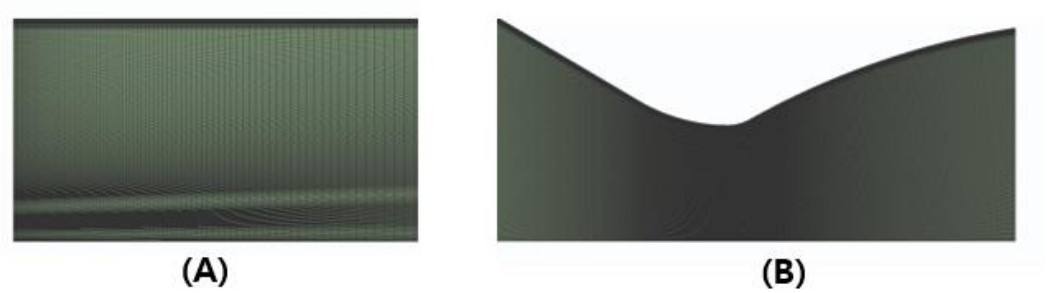

Figure 3: Enlarged view of the injector face region (A) and supersonic nozzle zone (B).

Figure 2 represents the grid system used for the entire computational domain, while Figure 3 provides an enlarged view of the grid in the injector inlet region and the supersonic nozzle. The grid system consists of a structured quadrilateral grid with a higher density of cells around regions where significant flow variations are expected. Prior to the calculations, a sensitivity analysis of the grid system was performed. The number of cells and nodes used in the grid system is summarized in Table 3, and Figure 4 compares the velocity distribution at the cross-section of nozzle exit for different grid resolutions. However, as shown in the table, the differences in error between each case were minimal. Therefore, in order to reduce the computational cost, the grid system with approximately 260,000 cells, referred to as the medium case, was used in the present calculations.

DOI: 10.13009/EUCASS2023-381

Table 3: Grid systems for the grid sensitivity analysis and the percentage error of thrust compared to the experiment results.

Case	Number of Cells	Number of Nodes	Error [%]
Coarse	134000	134871	0.86
Medium	263445	265647	0.23
Fine	452640	458475	0.16

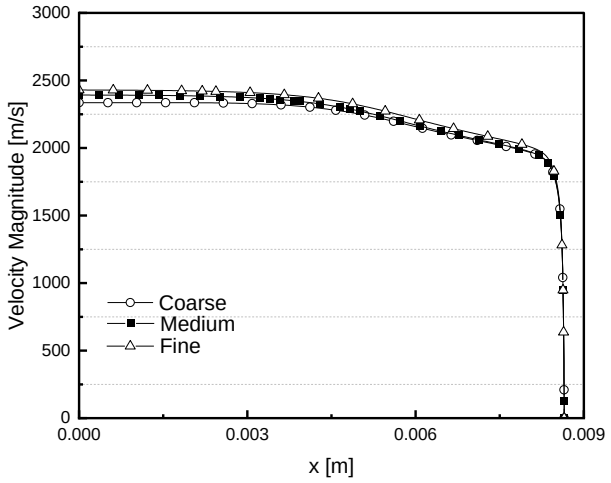

Figure 4: Velocity profiles along the cross-section of the nozzle exit.

4. Results and discussion

4.1 Steady state results

Before observing the flow structure of the combustion chamber, the numerical method was validated by calculating the thrust and combustion performance of the engine. The characteristic velocity is a standard of the engine's combustion performance and is defined by Eq. (6). The thrust is obtained by Eq. (7) consisting of contributions from momentum and pressure differences. In the calculation of thrust, the exhaust velocity and the pressure at the exit were obtained by mass-weighted average and area-weighted one over the nozzle exit, respectively.

$$C^* = \frac{P_c \cdot A_t}{\dot{m}_t} \tag{6}$$

$$F = \dot{m}_t \cdot v_e + (P_e - P_a)A_e \tag{7}$$

Figure 5 shows the characteristic velocity and its efficiency according to equivalence ratio for both period (I) and (II). It can be seen that the results in period (II) have lower percentage error compared to those in (I). This can be attributed to the fact that the values in period (II), which is at the later stage of the firing time, are closer to the steady state. The calculated thrust and chamber pressure from the analysis are compared and shown in Figure 6. It can be found that the combustion chamber pressure also shows an acceptable error, but for case GE1.x with equivalence ratio of 2, a difference in thrust occurs in both periods. It was confirmed that the abnormal thrust in the GE1.x case, was caused by a partial erosion of the combustor coming from the high flame temperature during the test.

DOI: 10.13009/EUCASS2023-381

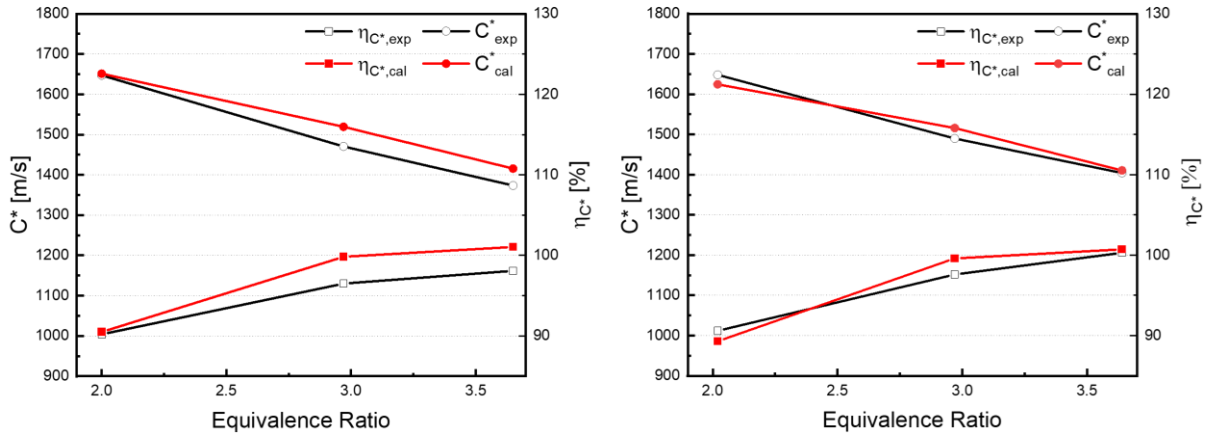

Figure 5: Comparison of the combustion performance between simulation and experiment results at period I (a) and period II (b).

Figure 7 presents the temperature distributions for each case. Overall, it can be observed that the flame extends up to the throat of the nozzle in all cases. Also, as the equivalence ratio increases, the flame region decreases, as does the maximum temperature. This is due to the increasing mass flow rate of methane, leading to the further deviation from the stoichiometric ratio, and thus to a weakening of the flame intensity.

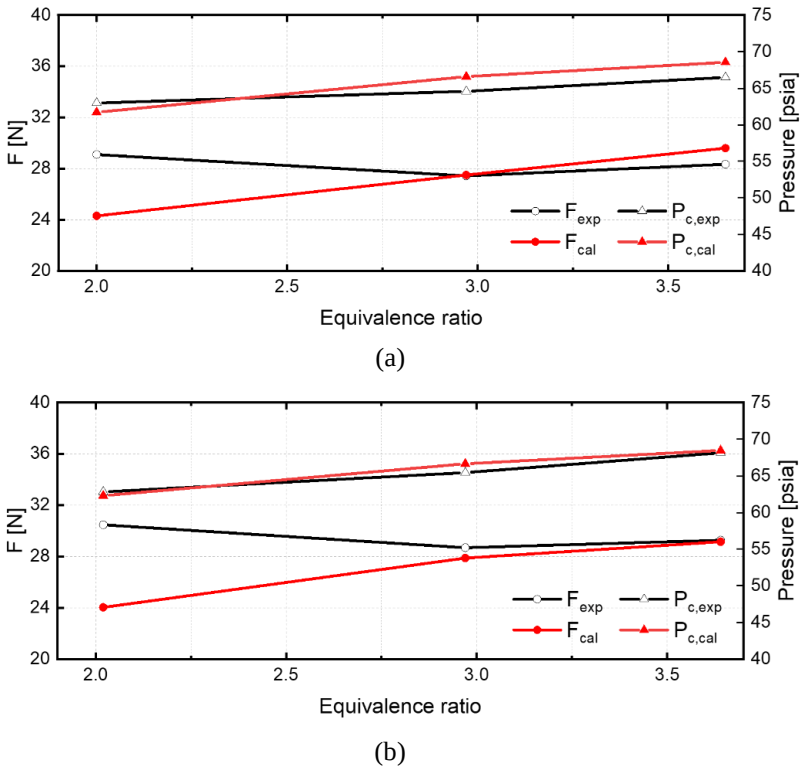

Figure 6: Comparison of the thrust and chamber pressure between simulation and experiment results at period I (a) and period II (b).

Figure 8 shows the magnitude of the heat flux at the combustor wall with varying the equivalence ratio. It is evident that the maximum heat load occurs near the nozzle throat in all cases. As observed from the temperature distribution, flame intensity increases near the nozzle throat, leads to a significant variation in heat flux at the same location.

DOI: 10.13009/EUCASS2023-381

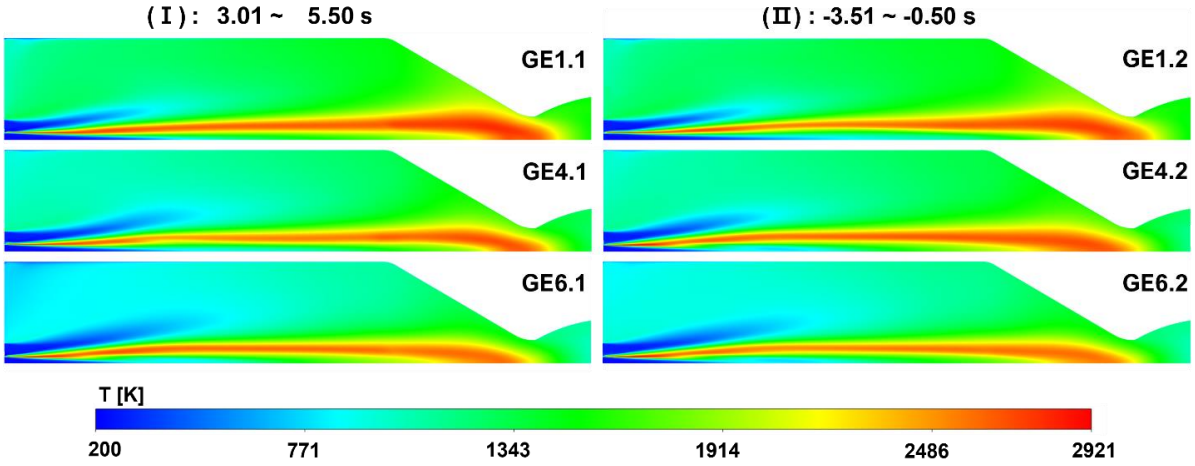

Figure 7: Temperature contour results at each case.

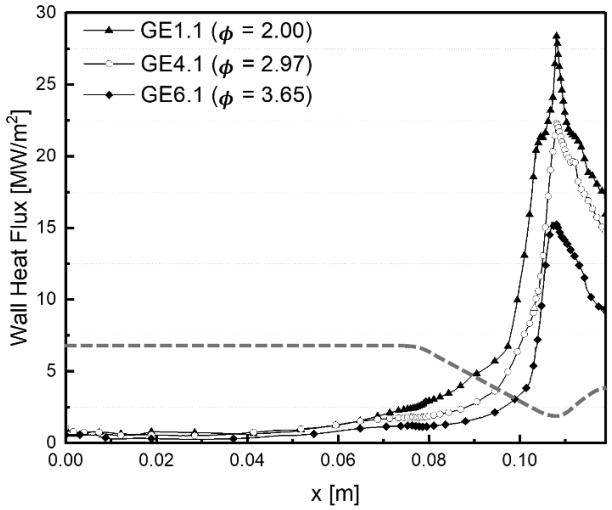

Figure 8: Wall heat flux distribution with equivalence ratio variation.

It can be also seen that the case with an equivalence ratio of 2 has a higher total heat load than others. Figure 9 presents the temperature contour along with streamlines to observe the recirculation zone inside the combustion chamber with equivalence ratio variation. Generally, the recirculation zone helps combustion efficiency be improved by enhancing the mixing of propellant within the combustion chamber[14]. In the figure, it is evident that as the mass-flow rate of methane increases, the recirculation zone within the combustion chamber expands, resulting in a reduction of high temperature region. This suggests that as the equivalence ratio increases, the fuel-rich region that does not participate in combustion may enlarge, raising the possibility of secondary ignition in this region during extended periods of combustion.

4.2 Transient state results

Figure 10 shows the results of the transient state analysis for the equivalence ratio of 5.36, where the change of characteristic velocity over time is highest. $P_{c,cal\ A}$ corresponds to the analysis result obtained by using the SIMPLEC algorithm, while $P_{c,cal\ B}$ corresponds to that by the pressure-based coupled algorithm. It is observed that the SIMPLEC algorithm generally overpredicts the pressure variation during the combustion process. Table 4 provides a summary of the results for thrust and characteristic velocity. As shown in the table, both methods exhibit higher error in the period (II), but the pressure-based coupled algorithm is closer to the experimental data. This indicates that the pressure-based coupled algorithm is more appropriate for calculating combustion processes with significant variations of the flow field.

DOI: 10.13009/EUCASS2023-381

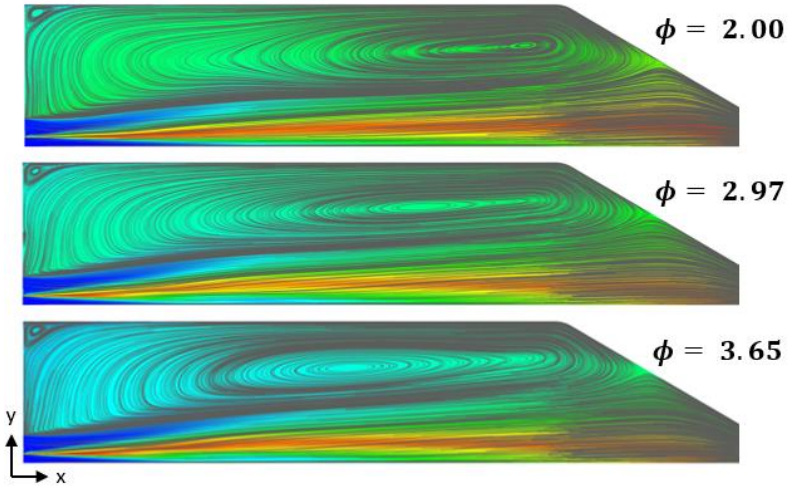

Figure 9: Comparison of recirculation zone in the combustion chamber with equivalence ratio variation

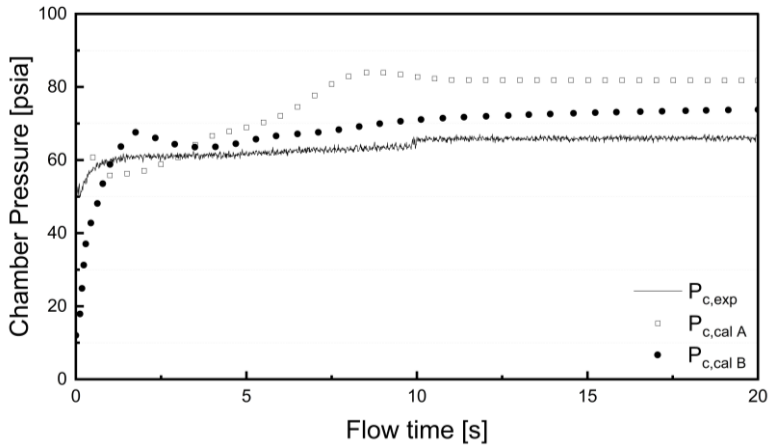

Figure 10: Comparison of chamber pressure over time between simulation and experiment results.

Meanwhile, an abrupt increase of pressure observed at the later part of practical firing was not clearly captured in the analysis. This can be attributed to a limitation of the combustion model, which has a difficulty to predict unsteady physics such as unburned mixtures re-entering the chemical reaction at the later period of combustion. Further research is supposed to be conducted for analyzing the flow structure in more detail by using combustion models such as finite rate and EDC (Eddy Dissipation Concept) in order to realize these real phenomena and also by refining the grid density in the recirculation zone.

Table 4: Comparison of characteristic velocity and thrust.

(I): EIG +3.01 ~ 5.50 s			
Case	**P_c [psia]**	**F [N]**	**C^* [m/s]**
Experiment	61.4	24.1	1045.7
SIMPLEC (A)	66.7	20.3	1135.8
Coupled (B)	64.3	24.4	1094.6
(II): ECO -3.51 ~ -0.50 s			
Case	**P_c [psia]**	**F [N]**	**C^* [m/s]**
Experiment	66.0	27.5	1115.8
SIMPLEC (A)	81.8	35.0	1392.4
Coupled (B)	73.5	30.6	1252.0

DOI: 10.13009/EUCASS2023-381

5. Conclusion

As part of a preliminary work, numerical analysis of GO_2-GCH_4 combustor was conducted in order to establish an analysis method for predicting combustion performance of liquid rocket engines. A non-adiabatic flamelet model was selected to simulate the turbulent flame field. And DRM-19 mechanism, which includes 21 chemical species and 84 reactions, were used for the analysis.

The equivalence ratio of 2 to 3.65 was analyzed in a steady state to observe the internal flame structure. It was found that the overall results show an acceptable error, but for case GE1.x with equivalence ratio of 2, a difference occurs in thrust. This is considered to be the uncertainty of the measured value due to the erosion of the combustion chamber caused by the high flame temperature during the test. In each case, it was shown that the flame intensity and the maximum heat load at the nozzle throat gradually decreased as the equivalence ratio increased. And it was observed that the recirculation zone expanded as the mass-flow rate of methane increased. This indicated that the fuel-rich region enlarged, raising the possibility of secondary ignition in this region during extended combustion periods.

To observe the abrupt increase of pressure over time in the equivalence ratio of 5.36, additional calculations were performed. As a result, it is confirmed that the pressure-based coupled algorithm was more appropriate than the SIMPLEC algorithm for calculating combustion processes with significant variations of the flow field. Meanwhile, an abrupt increase in pressure observed at the later part of practical firing was not captured in the analysis. This indicates a limitation of the combustion model in calculating of unsteady physics. To address this, further research will be conducted by varying with combustion model and refining the grid density in the recirculation zone.

6. Acknowledgements

This work was supported by the National Research Foundation (NRF) of Korea funded by the Ministry of Science and ICT under Grant (2022M1A3C2085070).

References

[1] Kim, J. S., Jung, H. and Kim, J. H. 2013. State of the Art in the Development of Methane/Oxygen Liquid-bipropellant Rocket Engine. *Journal of the Korean Society of Propulsion Engineers*. 174(6): 120-130.

[2] Goetz, A., Maeding, C., Brummel L. and Haeseler D. 2001. Application of non-toxic propellants for future launch vehicles. In: 37th AIAA/ASME/SAE/ASEE Joint Propulsion Conference & Exhibit. AIAA 2001-3546.

[3] Kang, Y. H., Ahn, H. J., Bae C. H. and Kim, J. S. 2021. Combustion Characteristics of the Gaseous-methane & Gaseous-oxygen Reactants under Highly Fuel-rich Conditions. Journal of the Korean Society of Propulsion Engineers. 25(6): 45-52.

[4] ANSYS Fluent Teory Guide, Release 21R1.

[5] Narayan, J. 1991. A two-equation turbulence model for compressible reacting flows. In : *29th Aerospace Sciences Meeting.* AIAA 1991-0755.

[6] Jones, W. P. and Launder, B. E. 1972. The prediction of laminarization with a two-equation model of turbulence. *International Journal of Heat and Mass Transfer.* 15(2): 301-314.

[7] Gerald J.M. and Helldorff, H. V. 2020. A Compressible Turbulence Model for High Speed Flows. Florida Institute of Technology. *Press*

[8] Fiuza, G. and Rezende, A. 2018. Comparison of k-ε Turbulence Model Wall Functions Applied on a T-Junction Channel Flow. *International Journal of Engineering Research & Science (IJOER)*. 4(1): 60-70

[9] Peters, N. 1984. Laminar diffusion flamelet models in non-premixed turbulent combustion. *Progress in Energy and Combustion Science*. 10(3): 319-339.

[10] Kim, G. H., Kim, H. J. and Kim, Y. M. 2005. Flamelet Modeling of Soot Formation and Oxidation in a laminar CH4-Air Diffusion Flame. *Journal of the Korean Society of Mechanical Engineers*. 13(1): 68-75.

[11] Chang, W. C. and Chen, J. Y. 1995. Reduced Reaction Sets based on GRI-Mech 1.2. from http://combustion. berkeley.edu/drm/drm19.dat

[12] Mazas, A. N., Fiorina, B., Lacoste, D. A. and Schuller, T. 2011. Effects of water vapor addition on the laminar burning velocity of oxygen-enriched methane flames. *Combustion and Flame*. 158(12): 2428-2440.

[13] McBride, B. J. and Gordon, S. 1996. Computer Program for Calculation of Complex Chemical Equilibrium Compositions and Applications, NASA Reference Publication 1311.

[14] Guessab, A., Aris, A., Cheikh, M. and T. Baki. 2016. Combustion of Methane and Biogas Fuels in Gas Turbine Can-type Combustor Model. *Journal of Applied Fluid Mechanics.* 9(5): 2229-2238.